Ab-initio Molecular-Dynamics Studies of the Effect of Solvation by Room-Temperature Ionic Liquids on the Vibrational Properties of a N719-Chromophore/Titania Interface

Aaron Byrne, Yogeshwaran Krishnan and Niall J. English*

School of Chemical and Bioprocess Engineering, University College Dublin, Belfield, Dublin 4, Ireland.

*E-mail: niall.english@ucd.ie

Abstract

The accurate *ab-initio* modelling of prototypical and well-representative photo-active interfaces for candidate dye-sensitised solar cells (DSCs) is a perennial problem in physical chemistry. To this end, using *ab-initio*, density functional theory (DFT)-based molecular dynamics (AIMD) has been carried out here to investigate the effect with which the choice of functional has on a system mimicking the essential workings of a DSC: the energetic properties of a $[bmim]^+[NTf2]^-$ room-temperature ionic liquid (RTIL), solvating a N719-sensitising dye adsorbed onto an anatase-titania (101) surface were scrutinised. In so doing, we glean important insights into how using a RTIL as the electrolytic hole acceptor alters and modulates the dynamical properties of the widely-used N719 dye. A fully crossed study has been carried out comparing the BLYP and PBE functionals, both unsolvated and solvated by the RTIL, both with and without Grimme D3 dispersion corrections. Also, vibrational spectra for the photo-active interface in the DSC configuration were calculated by means of Fourier-transforming atomic mass-weighted velocity autocorrelation functions. The *ab-initio* vibrational spectra were compared with high-quality experimental data and against each other; the effect of various methodological choices on the vibrational spectra were also studied, with PBE generally performed best in producing spectra which matched the experimental frequency modes typically expected.

Introduction

The band gap of semiconducting-substrate surfaces are modulated by photo-responsive dyes, which take in light and pass thereto, in dye-sensitised solar cells (DSCs). DSCs require that this transferred charge flux is recycled on a constant basis; thus, a redox electrolyte[1] is essential to the make-up of an organic solvent, such as I^-/I^{3-}.[2,3] In such a way, transfer of photo-excited, dye-originated holes to the electrolyte may be achieved, with resultant injected-charge passage into the substrate and onwards through the external circuit, with the electron-hole pair combining anew at the cathode; this is the basic *modus operandi* of a DSC. Crucially, DSCs' fabrication may be done without the need for materials of high purity, which is encouraging for boosting their outlook in a wide variety of real-world applications. The operational timeframes of DSCs may be lengthened a great deal by switching to use of electrolytes exhibiting lower volatility, with room-temperature ionic liquids (RTILs) constituting a leading exponent of such an electrolyte-substitution candidate. The electrical properties of RTILs are characteristic of those of a liquid, whilst their physical ones (such as low flammability, volatility and toxicity)[4] are redolent of a solid; this leads to RTILs being highly attractive as agents for usage in DSCs.

Given striking progress in Density Functional Theory (DFT)-based molecular simulation, particularly *ab-initio* molecular dynamics (AIMD), as an initial 'screening' technique in materials design, especially in the context of DSCs,[5-7] with critical assessment of optimal choice of functionals being *sine qua non*,[6,7] we have applied such approaches in to reveal important dispersion and solvation effects on both dye structure and binding modes at dye/substrate surfaces, with reasonable reproduction of essential electronic properties, such as band gap.[8-10] We have applied this extensively to a prototypical N719-chromophore adsorbed to an anatase-titania (101) interface, assessing vibrational and structural characteristics in the presence of a $[bmim]^+[NTf2]^-$ RTIL.[8,9] In particular, the structural rigidity of anatase (101), aside from its inherent relative photo-activity, means that the surface changes little during AIMD simulation, and is further motivation for the study of anatase (101) surfaces.[11] In ref. 8, we established that explicit dispersion interactions in RTIL-solvated systems led to the average separation between the cations and anions decreasing by 0.6 Å, the mean distance between the cations and the surface decreasing by about 0.5 Å and significant altering of the RTILs layering in the first layer surrounding the dye, with the cation being on average 1.5 Å further from the centre of the dye. Inclusion of explicit dispersion effects *in vacuo* resulted in unphysical kinking of the adsorbed

N719 dyes configuration. In ref. 9, we assessed as to whether these structural effect of explicit RTIL solvation and choice of functional affected the behaviour of the DSSCs, concluding that both explicit solvation and inclusion of dispersion is very important.

A compelling, and less addressed, question in the literature remains however, whether choices of the functional, dispersion and solvation affect more subtle properties of the system, such as adsorption energies and vibrational spectra, for which some previous high-quality benchmark simulation and experimental data is available for validation. Indeed, the present study sets out to explore whether choice of functional, dispersion and solvation is important to future work involving AIMD for these types of large, challenging *ab-initio* simulation systems from the viewpoint of energetic and vibrational properties.

The adsorption energy of the N719 dye onto titania surfaces has been estimated from statistical techniques. Previous state-of-the-art electronic-structure work by Mosconi *et al.*[12] has studied the effect which solvation by either water or acetonitrile has on the adsorption energy for three different acids, chosen so as to be reasonable substitutes for a full chromophore. The adsorption energy for the most stable configuration of benzoic acid was reported to be -0.03363, -0.02677 and -0.0215 Hartree for unsolvated, water- and actetonitrile- solvated systems, respectively. Similarly, the respective adsorption energies for the most stable configuration of 2-cyano-3-phenyl-acrylic acid were reported to be -0.03283, -0.02629 and -0.02837 Hartree for identical solvation conditions. By the same token, the corresponding respective energies for the most stable configuration of 4-(diphenylamino)-phenylcyanoacrylic acid were reported to be -0.03729, -0.0322 and -0.0260 Hartree. Mosconi *et al.*[12] demonstrated that the solvent played an important role in determining the stability of the dye on the anatase, which is of course vital for any design of DSC. Indeed, this motivates us in the present study to carry out a systematic, fully-crossed comparison BLYP and PBE[13] functionals for both RTIL-solvated and *in-vacuo* systems, with and without Grimme D3 dispersion corrections, to assess adsorption energy, as well as dynamical properties.

Even though the most widely used DFT functional are PBE and B3LYP[14], the decision was made to rule B3LYP out as a suitable candidate due to the work by Izgorodina *et al.*,[15] which showed that the B3LYP functional suffered from systematic errors in calculating the properties of ionic liquids. Hence, in the present work, we make a comparison for the N719-on-titania

system (with and without RTIL) between the two GGA functionals PBE (Perdew-Burke-Ernzerhof) and BLYP (Becke-Lee-Yang-Parr). In particular, bearing in mind that accurate far-infrared vibrational spectroscopy data for N719 is also available,[16,17] it is now timely to assess and validate the scope of DFT functionals, as well as to benchmark the inclusion of explicit dispersion treatment in functionals and gauge the importance of explicit solvation in AIMD studies on these more subtle and demanding adsorption-energy and vibrational properties,[18] having achieved some progress in understanding these effects in the context of gross structural properties.[8,9]

Methodology

The methodological simulation approach is adopted, by and large, from refs. 8 & 9, alongside some starting structures; much of this is outlined below for the reader's convenience. The N719 cis-di(thiocyanato)-bis(2,2'-bipyridl-4-carboxylate-4'-carboxylic acid)-ruthenium(II) dye, a well-studied prototype, was used for AIMD, in the absence of any counterions. Indeed, De Angelis *et al.*,[19] have found, after much detailed analysis, that this affords a good description of N719 bound to anatase-titania. Initially, N719 was adsorbed chemically to the TiO_2 surface through two carboxylate moieties, in a bi- and mono- dentate manner. This starting adsorbed configuration of the dye is similar to the configuration labelled as I1 determined by Schiffmann *et al.*,[20] in which they found it to be the most stable when surface protons were taken into account. The RTIL used in these simulations was 12 cation-anion pairs of 1-butyl-3 methylimidazolium bis(trifluoromethylsulfonyl)imide, $[bmim]^+[NTf2]^-$, consisting of 480 atoms. The starting configuration for the liquid was one that had been relaxed via classical molecular dynamics. The TiO_2 surface consisted of 288 atoms; it was imaged periodically along *x*- and *y*-laboratory axes (with lengths of 2.3 and 2.1 nm, respectively), projecting two parallel (101) surfaces to the RTIL under *z*-direction periodicity also. The DSC model with explicit solvent used in this study is composed of 827 atoms, with 4,300 valence electrons. For the '*in-vacuo*' case, there were 347 atoms and 2,530 valence electrons. These systems were simulated by BOMD using CP2K,[20-27] as described in refs. 8 & 9.

To provide for accurate assessment of how *in-vacuo* and explicitly-solvated treatments affect both adsorption energies and vibrational properties of the dye/substrate interface, six ~8.5-ps AIMD simulations were performed with a 1 fs time-step at 300 K in an NVT ensemble, with 400

Ry cut-off and triple-zeta basis sets with BLYP, BLYP-D, PBE and PBE-D functionals. For the simulations of systems including explicit dispersion effects (denoted by appending '-D'), Grimme-D3 dispersion corrections[28,29] were added to the functional. The temperature was fixed by coupling the systems to a Nosé-Hoover[30] thermostat with a period of 0.15 ps, and the virial-estimated[31] pressure was found to average to 1 atm. The six different AIMD simulations were run as below:

- BLYP system I; no dispersion corrections, no solvation.
- PBE system I; no dispersion corrections, no solvation.
- BLYP system II; no dispersion corrections, with [bmim][NTf_2] solvation.
- PBE system II; no dispersion corrections, with [bmim][NTf_2] solvation.
- BLYP system III; with dispersion corrections, with [bmim][NTf_2] solvation.
- PBE system III; with dispersion corrections, with [bmim][NTf_2] solvation.

Using AIMD trajectories, spectra were computed by Fourier-transforming each dye atom's velocity autocorrelation function (VACF), and weighting by each atom's mass and then summing these. This was done for VACFs extracted after the first 2 ps of simulation. This approach handles both temperature and anharmonicity effects, and extends readily into the far-infrared,[31-34] although it has been applied less commonly to systems of the relatively large present size before. In the same manner, the adsorption energies, and underlying standard errors, were estimated from data taken after 2 ps.

Results and Discussion

Relaxed Geometries and Binding Energies: Effects of Functional, Dispersion and RTIL Solvation

Representative configurations of the structure of the dye at the end of the six systems simulations can be seen from a frontal perspective in Fig. 1, with further details on structural properties in ref. 9 (*e.g.*, a comprehensive suite of pair distribution functions). PBE systems I shows explicit hydrogen bonding to the surface, with the PBE system undergoing (*in-vacuo*) the greatest changes to the dyes' initial binding modes.[9] In any event, none of the systems simulated with BLYP bend towards the surface to the same degree as that seen in the unsolvated PBE cases, although there is some tentative evidence of the BLYP system[9] beginning this process.

Also, the only simulation to exhibit a proton-transfer event from the surface to the dye was PBE system[9] which was simulated using PBE-D in the absence of ionic liquid. Evidence suggests that this setup then has the longest-range interactions of the systems studied;[9] indeed, this is not surprising, due to a comparative lack of charge shielding by vacuum in comparison to explicit solvent. All four of the systems solvated by $[bmim]^+[NTf2]^-$ remained stable throughout their trajectories, largely abetted by the solvation effects of the surrounding ionic liquid. Moreover, trajectory visualisation of the solvated systems showed no discernible difference vis-à-vis those simulated with the various functionals.

The adsorption energy of the N719 dye onto the bare (unsolvated) anatase surface was given by

$$E_{ads} = E_{slab\,\&\,dye} - E_{dye} - E_{slab} \quad (1)$$

and the various components of these BOMD-sampled energy calculations are reported in Table 1. As the energy components of the various systems were calculated from the combined energies of hundreds of atoms, it is expected that the central-limit theorem applies to each trajectory and the energies for each system are considered to be normally distributed. For samples with fewer data points it is ill-advised to perform an *F*-test for variances first, in order to determine whether the subsequent *t*-test should be the homoscedastic or heteroscedastic version.[35] Although most systems studied show reasonably similar adsorption-energy variances (SD ~ 0.01 - 0.02 Hartree), these are sufficiently different to require the usage of Welch's unequal-variance independent-sample *t*-test, which was carried out for all of the statistical comparisons in the present study. In any event, comparing BLYP (I) and PBE (I) for the bare-system case with the adsorption-energy data in Table 1, $t = 1.43$ and $p \sim 80\%$ for a two-tailed test, suggesting, strictly, no significant functional dependence in dye-binding energies (if one requires, say, 90+% to reject H_0). However, there is still a difference between BLYP and PBE that, even if not meeting a 90%-threshold to reject H_0 unambiguously), does serve to highlight the underlying differences in structural adsorption motifs encountered (cf. Figs. 1a versus 1b, and also ref. 9): in essence, the PBE I case's explicit hydrogen bonding to the surface enhances the binding-energy magnitude by some ~5% vis-à-vis BLYP (*i.e.*, -0.563 vs. -0.533 Hartree, cf. Table 1). This greatest PBE-case structural shift in the dye's initial binding modes[9] (cf. Fig. 1) leads to a (statistically) near-significant difference in adsorption energy; indeed, were the (very computationally expensive) AIMD simulations prolonged beyond ~8.5 ps, the greater mismatch between the binding-energy

estimates as time progresses clearly evident in Table 1 may well lead to a t-test indicating greater than 90% confidence to reject H_0 – a *de-facto* statistical-confidence standard in many aspects of physical chemistry.

For explicitly-solvated systems, the dye-adsorption energy was found by

$$E_{ads} = E_{slab\,\&\,dye\,\&\,RTIL} - E_{dye} - E_{slab\,\&\,RTIL} \quad (2)$$

BOMD-sampled components are detailed in Table 2. Eqn. 2 approximates the true adsorption energy: it neglects the energy required to create a cavity in the vacated space left by removing the dye in the $E_{slab\ \&\ RTIL}$ calculation. Still, this is a minor, second-order effect. Comparisons between BLYP and PBE for the RTIL-solvated case for adsorption-energy data in Table 2 using the unequal-variance *t*-test approach yields $t = 2.28$ and $p \sim 95\%$ for BLYP II vs. PBE II (*i.e.*, without dispersion) and $t = 0.20$ and $p \sim 17\%$ for III vs. III (*i.e.*, BLYP-D and PBE-D). Now, this indicates that, for explicit RTIL solvation, lack of Grimme-dispersion incorporation leads to a statistically significant difference between the BLYP and PBE functionals, whilst its inclusion in the DFT treatment essentially removes the difference. From a structural perspective, this stark disparity in explicit-solvation binding-energy outcomes/conclusions is reinforced dramatically from a structural standpoint by scrutiny in the first instance of Figs. 1c vs. 1d (*i.e.*, BLYP vs. PBE, *sans* Grimme), which show compelling evidence for the same PBE structural shift in the dye's initial binding modes as in Fig. 1b (for PBE without dispersion *in-vacuo*, see also ref. 9), with a near hydrogen-bond interaction evident to the anatase surface, identical to Fig. 1b. Indeed, similarly to the ~5% enhancement in without-dispersion binding-energy magnitude in favour of PBE vs. BLYP *in-vacuo* (*vide supra* and cf. Table 1), the RTIL-solvated augmentation is even greater at 9% in going from BLYP to PBE (*i.e.*, -0.620 vs. -0.569 Hartree, cf. Table 2). However, parallel comparison of Figs. 1e vs. 1f (*i.e.*, BLYP-D vs. PBE-D) shows that the PBE case no longer exhibits this strong electrostatic-interaction structural bending, interacting far less with the anatase surface. Therefore, inclusion of Grimme dispersion, when already solvated, suppresses this electrostatic-interaction propensity with the surface (a near hydrogen-bonding interaction), leading to essentially no difference between BLYP-D vs. PBE-D (cf. Table 2, and $t = 0.20$, *vide supra*).

To assess explicitly and quantitatively the effects of adding Grimme-dispersion interactions to the two GGA functionals, we compare for the explicitly-solvated cases PBE vs PBE-D (*i.e.*, PBE

II vs III) and *vice versa* for its BLYP counterpart. As discussed above, the inclusion of dispersion effects can produce noticeable differences in the structure of the interface (cf. Fig. 1 and ref. 9). Comparing PBE II vs III with binding-energy data from Table 2 leads to $t = 6.3$ and $p > 99\%$; for BLYP (i.e., II vs. III), we have $t = 8.5$ and $p >> 99\%$. The respective marginal tightening of binding energies are ~0.113 and 0.133 Ha. (roughly 3 and 4 eV, respectively). In the RTIL-solvated BLYP case, there is essentially double the augmentation in adsorption energy encountered as in the PBE situation, indicating the stronger differential impact of Grimme dispersion for the BLYP case; as seen above, this means that BLYP-D and PBE-D are very similar in adsorption energy and dye structure (see also Figs. 1e vs. 1f, and Table 2 for BLYP III vs. PBE III). In any event, we have seen the dramatic effect of inclusion of explicit dispersion *per se* in the more realistic case of RTIL solvation (with ref. 9 discussing primarily structural aspects of dispersion inclusion *in-vacuo*): it leads to tighter dye binding for both GGA functionals, although - reassuringly - essentially serves to eliminate the major structural and energetic differences between them when present.

The study of how explicit RTIL solvation *per se* alters binding energy quantitatively may be accomplished by comparison of bare (I) and solvated systems (II) in the absence of explicit dispersion interactions. To this end, binding-energy comparison (with data from Tables 1 & 2) leads to $t = 1.4$ and $p \sim 80\%$ and $t = 2.5$ and $p \sim 95\%$ for two-tailed tests for BLYP and PBE, respectively, with respective tighter binding by roughly 0.035 and 0.055 Ha (if the order of 1 and 1.5 eV). Therefore, there is a strong effect of solvation I both cases, with PBE being more dramatic (with some further enhancement of the Coulombic interaction in the surface, cf. Figs. 1b vs 1d and see also ref. 9). Although the BLYP case does not exhibit strictly statistical significance at quite the 90%-confidence threshold, comparison of the time evolution of the BLYP I & II adsorption-energy estimates in Tables 1 & 2 makes it clear that a longer run of these very computationally-demanding simulations would most probably lead to a statistically significant difference within several more picoseconds (*i.e.*, with a *t*-test indicating 90%-or-more confidence level). With that in mind for both functionals, this constitutes a rather stark and dramatic example of the effect of explicit solvation in the estimation of energetic and structural properties for DFT-based MD; these findings is in agreement for the presently-studied N719 dye with those for a ruthenium-based H_2-storage catalyst also scrutinised for structure and energetics with respect to explicit solvation.[36]

Vibrational Spectra: Effects of Solvation, Functional and Dispersion

Each of the plotted mass-weighted spectra in this section (cf. Figs. 2 & 3) can be interpreted as follows: the continuous coloured line is the vibrational spectra generated from BOMD between 0 and 2500 cm^{-1}. N719 experimental modes are depicted at 1230, 1380, 1450, 1540, 1600, 1720 and 2100 cm^{-1}. The two grey spectral insets are experimental results from ref. 16 with the topmost for gas-phase N719 and the bottom one being the unsolvated dye powder on anatase. Now, it must be emphasised that the experimental modes are intended purely as a qualitative guide; indeed, the spectra are slightly different in other studies and the two experimental insets vary between themselves, attributable to anatase-binding. These experimental results are meant as a guide only, as the spectra are slightly different in other studies and the two experimental insets themselves are quite different due to the inclusion of the anatase and N719 binding thereon. A solvent's presence, whether acetonitrile or an RTIL, will sever to change spectra. Further, experimentally-measured spectra possess a more restricted frequency range, and represent an amalgamation of the dynamics of multiple dyes in various geometries in contrast, our BOMD is for a single surface-bound dye, with a more defined resultant spectrum.

For PBE, overall, the experimental modes of the *in-vacuo* spectra in Fig. 2 are reproduced by AIMD with reasonable fidelity. The thiocyano-moiety 2100 cm^{-1} peak is modulated and moved to 2000 cm^{-1}, the 1600 cm^{-1} mode is weaker than experiment, whilst the 1230 cm^{-1} peak is blue-shifted to 1280 cm^{-1}. Despite these disparities, the other modes are in excellent accord between the experimental and simulated spectra. A few far-IR of modes (< 500 cm^{-1}) differ between the PBE spectra: this is likely to be attributable to the various different binding motifs which the dyes adopt, in the end. In the case of BLYP, there is good accord in terms of prediction of mode frequencies vis-à-vis experiment,[16] except for the large peak at 1500 cm^{-1}. BLYP system I, which does not have additional dispersion corrections added, appears to align well, in-vacuo, with the established experimental-IR vibrational modes.[16,17] In comparing the unsolvated-dye spectra on anatase, we found that PBE (system I) agreed more closely with the experimental peaks than BLYP (I), although the 1230 cm^{-1} peak was better captured by BLYP system I (cf. Fig. 2).

Fig. 3 shows the spectra for the explicitly-solvated systems. Here, one may gauge dispersion effects on GGA functionals, in terms of dynamical properties of the $[bmim]^+[NTf2]^-$-solvated dyes. In the case of BLYP, it is interesting to note that in terms of the relative magnitude of the

peaks, BLYP II (*sans* Grimme) resembles the experimental signal without anatase, and BLYP III (*i.e.*, BLYP-D, with dispersion) resembles the signal with anatase. This indicates that for the solvated systems, BLYP with dispersion enhances the effect which anatase has on the frequencies of the dye. This may be rationalised by longer-range dispersion contributions afforded by BLYP, allowing the titania surface to couple more closely with the dynamics of the dye.[7] The far-IR structure for the two BLYP systems (with and without dispersion) agree closely with one another, indicating that this part of the spectra depends strongly on the geometry of the dye. In the unsolvated systems, we did not see this sort of close agreement upon addition of dispersion to the functional; however, with the surrounding solvent included, the structure remains more 'upright' and the location of the peaks in the region < 1000 cm^{-1} align closely.

The PBE system III spectra (*i.e.*, with dispersion and explicit solvation, cf. Fig. 3d), resembles closely the N719 spectrum from experiment; even the thiocyano N-C moiety's peak at 2100 cm^{-1} is reproduced. Naturally, displacement of modes with respect to experiment is evident, although this would not be unexpected in the present work, given the explicit solvation of N719 by the RTIL in simulations as opposed to a dry dye in experiment. The largest peak displacement takes place for the 1230 cm^{-1} mode, which is blue-shifted to 1300 cm^{-1}. Again, some peaks for the PBE-II system (without dispersion) are shifted due to the presence of the solvent, and, overall, the PBE-II spectra are very similar to those of PBE III (with dispersion), although the relative intensities of modes in the far-IR region is somewhat different between the two systems.

None of the three BLYP cases simulated in the present work has a strong vibrational mode at 1720 cm^{-1} associated with the carboxylic-acid moiety. In the case of PBE, only system II (explicit solvation, without Grimme) does not have a strong vibrational mode here. This particular mode depends upon the coupling of the carboxylic acid to the anatase surface, which dispersion corrections naturally serve to enhance. This finding supports further two previous hypotheses: firstly, the BLYP functional has less inherent longer-range effect than PBE, and, secondly, solvation serves to reduce the effect that dispersion corrections have on the system by damping the longer-range interactions.

The modes of the PBE spectra are generally shifted to higher frequencies than the same modes in the BLYP spectra. For explicit solvation without Grimme PBE II performs better at reproducing the experimental modes over 1300 cm^{-1}, whereas BLYP II captures the 1230 cm^{-1}

mode with greater quantitative accuracy. Upon inclusion of explicit dispersion, this is also true for comparison between PBE III and BLYP III, with the spectra from PBE III having peaks closest to the established experimental modes[10,11] of any of the systems studied. The PBE-D system (III) generally does a good job of capturing the thiocyano mode, and is also the only RTIL-solvated system to exhibit the carboxylic-acid mode, therefore showing combined qualitative superiority for all of the DFT and solvation treatments studied in the present work.

Conclusions

In expensive BOMD simulation of RTIL-solvation effects on N719 vibrational spectra adsorbed to anatase-titania interfaces, as well as adsorption energies thereon, we have compared PBE against another GGA functional, BLYP, as well as the use of Grimme-D3 dispersion, building on previous studies of refs. 8 & 9 on, *inter alia*, structural properties. With respect to the structure of the anatase surface itself, solvation by RTIL had marked effects, with the titania interface exhibiting stability throughout, as well as enhancing the rigidity of the N719's carbon-backbone 'skeleton'.

The PBE-simulated systems generally perform better in reproducing the thiocyano-associated spectral modes than do the BLYP systems. In the far-IR spectral region, the geometry of the dye relative to the anatase plays an important role; additional dispersion interactions can affect this, in so far as they alter the relaxed geometry of the dye (cf. Fig. 1 and ref. 9). For both the BLYP and PBE systems, addition of dispersion corrections for explicitly-solvated systems results in a change to the relative magnitude of the frequency modes, but does not cause substantial shifting of the various underlying modes' locations. The effect of solvation on the dynamical properties of the dyes changes the magnitude of frequency modes relative to each other and also causes some of the modes to be shifted by about 50 cm^{-1} towards higher frequencies. However, spectral similarities emerge in the vibrational features of all of the analysed solvated systems. Naturally, different binding motifs lead to altered spectra, as is dramatically evident by the relative magnitudes of the carboxylic versus the carboxylate modes in Fig. 3, which originate from two or three binding modes.[9] In terms of the RTIL-solvated cases, PBE-D (*i.e.*, PBE III) offers clearly superior performance in producing spectra which match the expected experimental frequency modes.

In terms of dye-adsorption energies, it was found that explicit solvation and dispersion tended to have statistically significant effects upon their incorporation into BOMD simulation, mirroring structural changes in dye-substrate interactions upon their usage (cf. Fig. 1 and ref. 9). It was found that the impact solvation was more dramatic in the case of the PBE functional on the binding energy, mirroring the earlier structural findings of ref. 9. In general terms, bearing in mind both energetic and dynamical properties studied in detail in the present work, as well as structural aspects in ref. 9, the effects of explicit solvation on energetic, structural and dynamical properties have been shown to require careful treatment in DFT with N719 dyes, and especially in AIMD. This mirrors findings, as mentioned previously, with those in our earlier work for a ruthenium-based H_2-storage catalyst, where we found dramatic explicit-solvation effects on structure, vibrational properties and energetics.[36] Therefore, future work by the DFT and AIMD simulation community needs to validate carefully and appraise critically the accuracy of both functionals and treatment of dispersion, as well as solvation strategies.

Acknowledgements

The authors thank Prof. David Coker for useful discussions and the Irish Centre for High-End Computing (ICHEC) and Science Foundation Ireland (SFI) for the provision of High-Performance Computing resources. This research has been supported by the SFI-NSFC bilateral funding scheme (grant number SFI/17/NSFC/5229), as well as the Programme for Research in Third Level Institutions (PRTLI) Cycle 5, cofunded by the European Regional Development Fund. This project has received funding from the European Union's Horizon 2020 research and innovation programme under grant agreement No. 643998.

References

(1) Labat, F.; Ciofini, I.; Hratchian, H. P.; Frisch, M.; Raghavachari, K.; Adamo, C. First Principles Modeling of Eosin-Loaded ZnO Films: A Step toward the Understanding of Dye-Sensitized Solar Cell Performances. *J. Am. Chem. Soc* **2009**, 131, 14290–14298.

(2) Labat, F.; Bahers, T. L.; Ciofini, I.; Adamo, C. First-Principles Modeling of Dye-Sensitized Solar Cells: Challenges and Perspectives. *Acc. Chem. Res* **2012**, 45, 1268–1277.

(3) Bahers, T. L.; Pauporté, T.; Laine, P. P.; Labat, F.; Adamo, C.; Ciofini, I. Modeling Dye-Sensitized Solar Cells: From Theory to Experiment. *J. Phys. Chem. Lett* **2013**, 4, 1044-1050.

(4) Ohno, H. *Electrochemical Aspects of Ionic Liquids*; John Wiley & Sons, **2011**.

(5) Agrawal, S.; English, N. J.; Thampi, K. R.; MacElroy, J. M. D. Perspectives on Quantum-Based Molecular Simulation of Excited-State Properties of Organic Dye Molecules in Dye-Sensitised Solar Cells. *Phys. Chem. Chem. Phys* **2012**, *14*, 12044-12056

(6) Agrawal, S.; Dev, P.; English, N. J.; Thampi, K. R.; MacElroy, J. M. D. A TD-DFT Study of the Effects of Structural Variation on the Photo-Chemistry of Polyene Dyes. *Chem. Science* **2012**, *3*, 416-424

(7) Dev, P.; Agrawal, S.; English, N. J. Functional Assessment for Predicting Charge-Transfer Excitations of Dyes in Complexed State: A Study of Triphenylamine-Donor Dyes on Titania for Dye-Sensitized Solar Cells. *J. Phys. Chem. A* **2013**, *117*, 2114-2124

(8) Byrne, A.; English, N. J.; Schwingenschlogl, U.; Coker, D. F. Dispersion and Solvation Effects on the Structure and Dynamics of N719 Adsorbed to Anatase- Titania Surfaces in Room-Temperature Ionic Liquids: An *ab-Initio* Molecular Simulation Study. *J. Phys. Chem. C* **2016**, *120*, 21-30

(9) Byrne, A.; and English, N. J. A Systematic Study via *ab-Initio* MD of the Effect Solvation by Room Temperature Ionic Liquid has on the Structure of a Chromophore-Titania Interface. *Comput. Mater. Sci.* **2018**, *141*, 193–206.

(10) Snaith, H. J. Estimating the Maximum Attainable Efficiency in Dye-Sensitized Solar Cells. *Adv. Funct. Mater.* **2010**, 20, 13–19.

(11) Hengerer, R.; Bolliger, B.; Erbudak, M.; Grätzel, M. Structure and Stability of the Anatase TiO_2 (101) and (001) Surfaces. *Surf. Sci.* **2000**, *460*, 162–169.

(12) Mosconi, E.; Selloni, A.; De Angelis, F. Solvent Effects on the Adsorption Geometry and Electronic Structure of Dye-Sensitized TiO2: a First-Principles Investigation. *J. Phys. Chem. C* **2012**, *116*, 5932–5940.

(13) Perdew, J. P.; Burke, K.; Ernzerhof, M. Generalized Gradient Approximation Made Simple *Phys. Rev. Lett.* **1996**, 77, 3865-3868.

(14) Kim, K.; Jordan, K. D. Comparison of Density Functional and MP2 Calculations on the Water Monomer and Dimer. *J. Phys. Chem.*, **1994**, 98 (40), pp 10089–10094.

(15) Izgorodina, E. I.; Bernard, U. L.; MacFarlane, D. R. Ion-pair Binding Energies of Ionic Liquids: Can DFT Compete with *ab-Initio* Based Methods? *J. Phys. Chem. A* **2009**, *113*, 7064-7072.

(16) León, C. Vibrational Spectroscopy of Photosensitizer Dyes for Organic Solar Cells; Cuvillier, **2006**.

(17) Finnie, K. S.; Bartlett, J. R.; and Woolfrey, J. L. Vibrational Spectroscopic Study of the Coordination of (2, 2'-bipyridyl-4, 4'-dicarboxylic acid) Ruthenium (II) Complexes to the Surface of Nanocrystalline Titania. *Langmuir* **1998**, *14*, 2744-2749.

(18) Krishnan, Y.; Byrne, A.; English, N. J. Vibrational Study of Iodide-Based Room-Temperature Ionic-Liquid Effects on Candidate N719-Chromophore/Titania Interfaces for

Dye-Sensitised Solar-Cell Applications from Ab-Initio Based Molecular-Dynamics Simulation. *Energies* **2018**, *11*, 2570.

(19) De Angelis, F.; Fantacci, S.; Selloni, A.; Nazeeruddin, M. K.; Grätzel, M. J. First-Principles Modeling of the Adsorption Geometry and Electronic Structure of Ru (II) Dyes on Extended TiO_2 Substrates for Dye-Sensitized Solar Cell Applications. *Phys. Chem. C* **2010**, *114*, 6054-6061.

(20) Schiffmann, F.; VandeVondele, J.; Hutter, J.; Wirz, R.; Urakawa, A.; Baiker, A. J. Protonation-Dependent Binding of Ruthenium Bipyridyl Complexes to the Anatase Surface. *Phys. Chem. C* **2010**, *114*, 8398-8404.

(21) Lippert, G.; Hutter, J.; and Parrinello, M. A Hybrid Gaussian and Plane Wave Density Functional Scheme. *Mol. Phys.* **1997**, *92*, 477-488.

(22) VandeVondele, J.; Krack, M.; Mohamed, F.; Parrinello, M.; Chassaing, T.; and Hutter, J. Quickstep: Fast and Accurate Density Functional Calculations Using a Mixed Gaussian and Plane Waves Approach. *Comput. Phys. Commun*. **2005**, *167*, 103-128.

(23) VandeVondele, J.; Hutter, J. An Efficient Orbital Transformation Method for Electronic Structure Calculations. *J. Chem. Phys.* **2003**, *118*, 4365-4369.

(24) Lippert, G.; Hutter, J.; Parrinello, M. The Gaussian and Augmented-Plane-Wave Density Functional Method for *ab-Initi*o Molecular Dynamics Simulations. *Theor. Chem. Acc.* **1999**, *103*, 124-140.

(25) Krack, M.; Parrinello, M. All-Electron *ab-Initio* Molecular Dynamics. *Phys. Chem. Chem. Phys.* **2000**, *2*, 2105-2112.

(26) Grotendorst, J. High-Performance Computing in Chemistry; John von Neumann Institute for Computing, **2004**.

(27) Hutter, J.; Iannuzzi, M.; Schiffmann, F.; VandeVondele, J. CP2K: Atomistic Simulations of Condensed Matter Systems. *Wiley Interdiscip. Rev. Comput. Mol. Sci.* **2014**, *4*, 15-25.

(28) Grimme, S.; Antony, J.; Ehrlich, S.; and Krieg, H. A Consistent and Accurate *ab-Initio* Parametrization of Density Functional Dispersion Correction (DFT-D) for the 94 Elements H-Pu. *J. Chem. Phys.* **2010**, *132*, 154104.

(29) Grimme, S. Semi-Empirical GGA-Type Density Functional Constructed with a Long-Range Dispersion Correction. *J. Comput. Chem.* **2006**, *27*, 1787-1799.

(30) Hoover, W. G. Canonical dynamics: Equilibrium Phase-Space Distributions. *Phys. Rev. A* **1985**, *31*, 1695.

(31) Allen, M. P.; Tildesley, D. J. Computer Simulation of Liquids; Oxford University Press, **1989**.

(32) Thomas, M.; Brehm, M.; Fligg, R.; Vöhringer, P.; Kirchner, B. Computing Vibrational Spectra from *ab-Initio* Molecular Dynamics. *Phys. Chem. Chem. Phys.* **2013**, *15*, 6608-6622.

(33) Mancini, J. S.; Bowman, J. M. On the *ab-Intitio* Calculations of Anharmonic Vibrational Frequencies: Local-Monomer Theory and Application to HCl Clusters. *J. Chem. Phys.* **2013**, *139,* 164115.

(34) Jaeqx, S.; Oomens, J.; Cimas, A.; Gaigeot, M.-P.; Rijs, A.M. Gas-Phase Peptide Structures Unraveled by Far-IR Spectroscopy: Combining IR-UV Ion-Dip Experiments with Born-Oppenheimer Molecular-Dynamics Simulations, *Angew. Chem.* **2014**, *126,* 3737-3740.

(35) Sawilowsky, S. S. Fermat, Schubert, Einstein, and Behrens-Fisher: The Probable Difference Between Two Means When $\sigma_1^2 \neq \sigma_2^2$, *J. Modern App. Stat. Methods* **2002**, *1,* 461–472.

(36) Bandaru, S; English, N. J.; MacElroy, J. M. D. Implicit and Explicit Solvent Models for Modelling a Bifunctional Arene Ruthenium Hydrogen-Storage Catalyst: a Classical and *ab-Initio* Molecular Simulation Study, *J. Comput. Chem.* **2014**, *35***,** 683-691.

Table 1: Energy terms (Hartrees) in eqn. 1 for unsolvated cases over 2-8 ps in 2-ps segments, with means and standard deviations

E_{slab}	BLYP I	PBE I
2-4 ps	-8677.517	-8681.661
4-6 ps	-8677.552	-8681.700
6-8 ps	-8677.584	-8681.710
Mean	-8677.551	-8681.690
SD	0.0335	0.0259
E_{dye}		
2-4 ps	-458.909	-459.851
4-6 ps	-458.932	-459.861
6-8 ps	-458.903	-459.845
Mean	-458.915	-459.852
SD	0.0153	0.0081
$E_{slab\&dye}$		
2-4 ps	-9136.987	-9142.089
4-6 ps	-9136.995	-9142.116
6-8 ps	-9137.017	-9142.112
mean	-9136.99	-9142.106
SD	0.0155	0.0146
$E_{ads.}$		
2-4 ps	-0.560	-0.577
4-6 ps	-0.511	-0.555
6-8 ps	-0.530	-0.558
mean	-0.533	-0.563
SD	0.0248	0.0119

Table 2: Energy terms (Hartrees) in eqn. 2 for solvated systems over 2-8 ps in 2-ps segments, with means and standard deviations

$E_{slab/RTIL}$	BLYP II	PBE II	BLYP III	PBE III
4 ps	-12578.16	-12588.45	-12581.97	-12590.35
6 ps	-12578.08	-12588.43	-12582.03	-12590.31
8 ps	-12578.15	-12588.39	-12582.00	-12590.41
mean	-12578.13	-12588.43	-12582.00	-12590.36
SD	0.0286	0.0223	0.0510	0.0413
E_{dye}				
4 ps	-458.89	-459.86	-459.00	-459.89
6 ps	-458.90	-459.86	-459.01	-459.90
8 ps	-458.91	-459.84	-459.02	-459.90
Mean	-458.90	-459.85	-459.01	-459.89
SD	0.0164	0.0085	0.0104	0.0047
$E_{Slab/Dye/RTIL}$				
4 ps	-13037.57	-13048.90	-13041.72	-13050.96
6 ps	-13037.56	-13048.87	-13041.74	-13050.96
8 ps	-13037.63	-13048.88	-13041.76	-13051.03
mean	-13037.58	-13048.88	-13041.74	-13050.98
SD	0.0367	0.0226	0.0234	0.0322
E_{ads}.				
4 ps	-0.525	-0.597	-0.757	-0.728
6 ps	-0.577	-0.586	-0.703	-0.752
8 ps	-0.573	-0.649	-0.730	-0.719
Mean	-0.569	-0.620	-0.730	-0.733
SD	0.0203	0.0296	0.0221	0.0146

Figure Captions

Fig. 1: Frontal view showing the relaxed geometries of the BLYP and PBE systems. Carbon shown in dark grey, nitrogen in dark blue, oxygen in red, hydrogen in white, titanium in light grey, sulphur in yellow and ruthenium in light green. System types; I: unsolvated, II: solvated with [bmim][NTf2] , III: solvated with [bmim][NTf2] with dispersion corrections. Solvated systems are shown without solvent, for ease of viewing.

Fig. 2: Vibrational spectra of (a) BLYP system I, (b) PBE system I. Within each plot, the grey (lower) / (upper) inset corresponds to the experimental ATR-FTIR signal from ref. 16 for (dry-N719 adsorbed onto anatase) / (dry-N719 powder). The dashed lines indicate established vibrational modes.[17]

Fig. 3: Vibrational spectra of (a) BLYP system II, (b) PBE system II, (c) BLYP system III, and (d) PBE system III. In each plot, the grey (lower) / (upper) inset corresponds to the experimental ATR-FTIR signal[16] for (dry-N719 adsorbed onto anatase) / (dry-N719 powder). Dashed lines indicate established vibrational modes.[17]

(a) BLYP System Type I

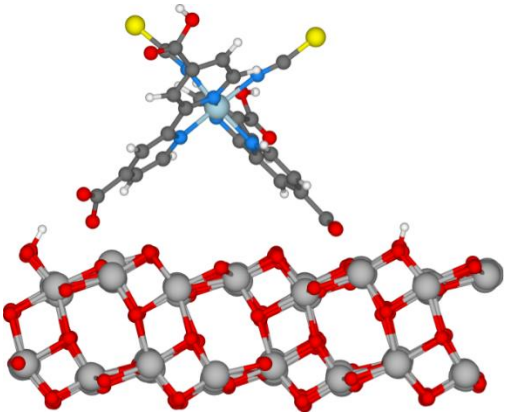

(b) PBE System Type I

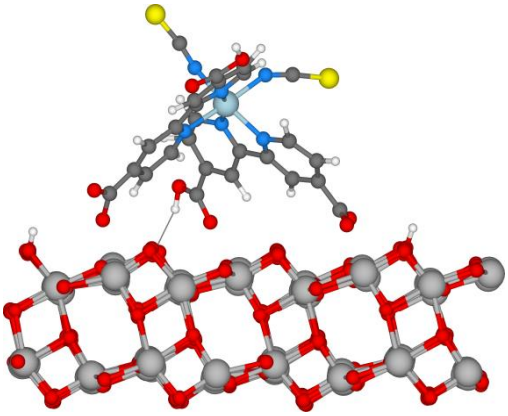

(c) BLYP System Type II

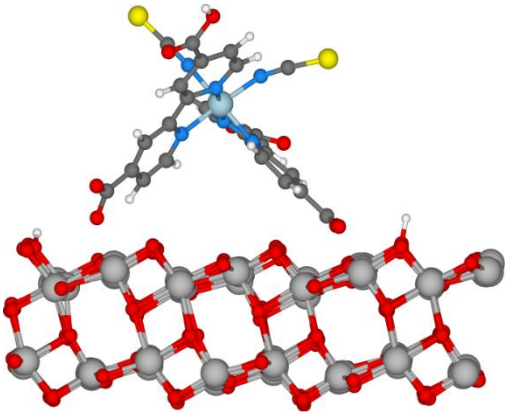

(d) PBE System Type II

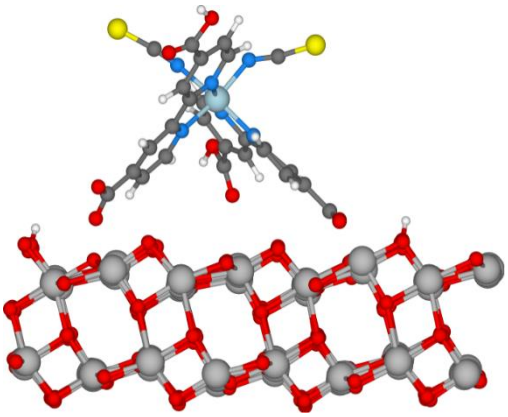

(e) BLYP System Type III

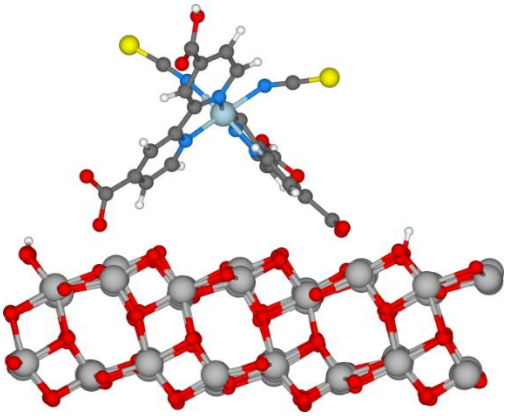

(f) PBE System Type III

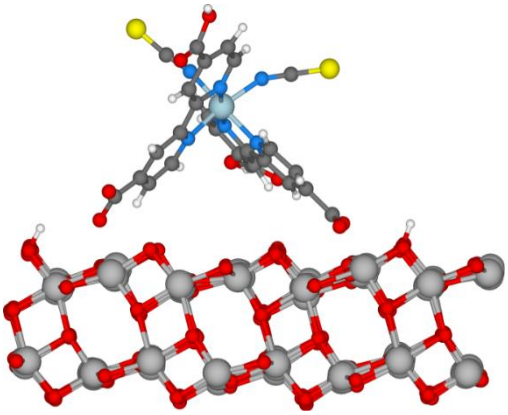

Fig. 1

(a) BLYP System Type I

(b) PBE System Type I

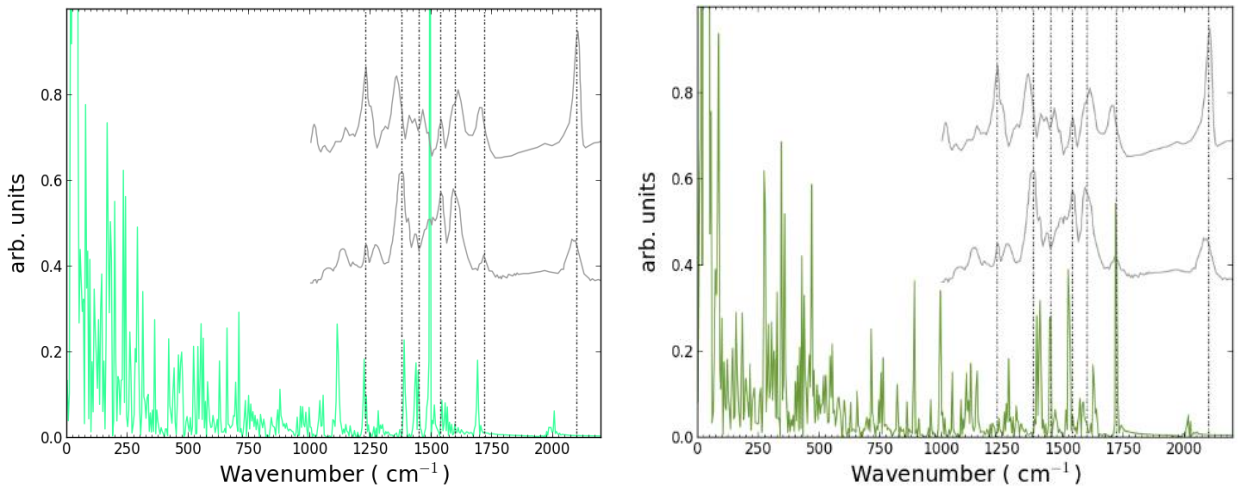

Fig. 2

(a) BLYP System Type II

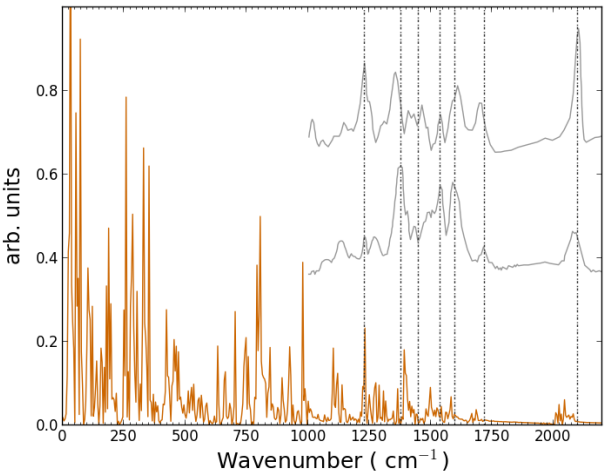

(b) PBE System Type II

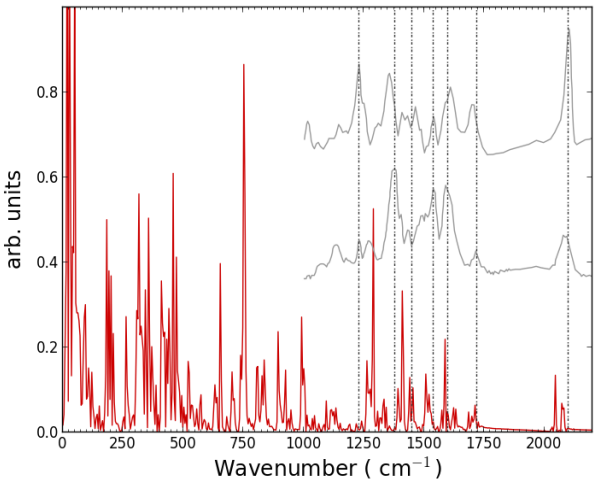

(c) BLYP System Type III

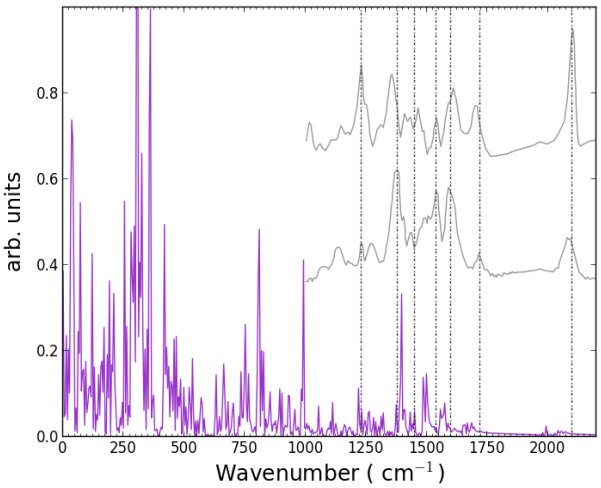

(d) PBE System Type III

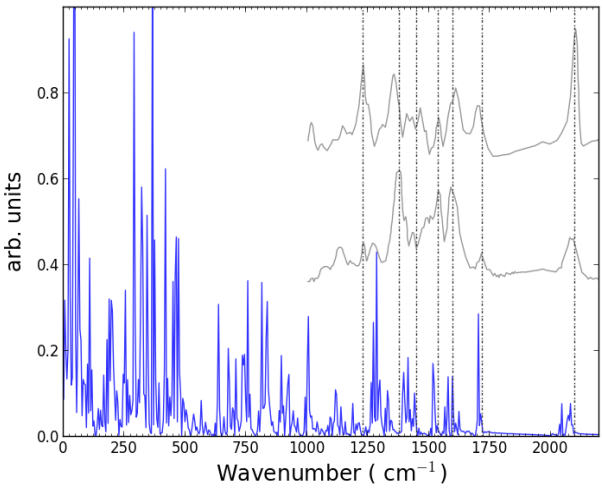

Fig. 3

TOC Image